Transport of hierarchical porous materials: Diffusion experiments and random walk simulations

Véronique Wernert, Benoit Coasne, Pierre Levitz, Khac Long Nguyen, Edder Garcia, Renaud Denoyel

Transport in hierarchical porous materials:

diffusion experiments and random walk simulations

V. Wernert, B. Coasne, P. Levitz, K. Nguyen, E.J. Garcia, R.Denoyel.

Abstract. We carry out random walk simulations on prototypical porous structures that are representative of actual hierarchical silica-based materials. The main throughput of the mesoscopic simulations proposed here is the tortuosity defined as the ratio of the fluid mean square displacements calculated in the absence and in the presence of the porous medium. This is a rigorous mathematical definition that has the advantage to be comparable to the ratio of self-diffusion coefficients for the bulk and confined fluid, which can be directly determined by means of diffusion experiments. Such tortuosity can also be compared with the ratio of bulk and effective electrical conductivities. These calculations are applied here to hierarchical materials such as those encountered in chromatography, membrane science or catalysis. The simulation results are compared to experimental data as well as to effective equations – such as Maxwell's equation – which are often invoked to infer tortuosity expressions based on effective mean field theories.

1. Introduction

Understanding the role of porous material morphology on the transport properties of a fluid is central to many natural and engineering processes.[1] This scientific issue is at the heart of many fields (geology, engineering, chemistry, and physics) with important applications such as catalysis, separation, cement chemistry, etc.[2] The modeling of experimental results, for example peaks in chromatography or breakthrough curves, requires a large number of input parameters for a set of equations that describe flow properties, chemical reactions at interfaces, and diffusion. Generally, such an equation set is only well defined at a given time/length scale; it is therefore necessary to establish the coupling rules between the different scales. This is done for example in the General Rate Model in chromatography which simplifies the approach by considering that liquid flow only occurs in macropores whereas diffusion occurs everywhere.[3,4] To be understood and modelled, the apparent diffusion in the whole system should be deduced from the diffusion contributions in each pore domain i.e. scale.[5] This can be done easily by assuming that domains are either in parallel or in series but, except perhaps in the case of membranes made of several layers that can be considered in a serial arrangement, the actual situation is rather complex and cannot be described so simply. This is why Effective Medium Theory (EMT) models were proposed to describe the properties of heterogeneous systems[6] with an expected better approximation than parallel or series arrangements. Maxwell's equation is for example used in the field of chromatography[7,8] to relate the overall effective diffusion to the diffusion in the different parts of the column.

Regardless of their structure, compact beds of spherical particles or monoliths with a skeleton defining macroporous and mesoporous domains, chromatographic columns are typical hierarchical porous media where the arrangement of domains is optimized for efficient transport. In this context, hierarchy means that pores are organized in such a way that domains can be identified in terms of pore size, porosity and space arrangement but the system appears homogeneous at the macroscale. It is then interesting to test the applicability of Maxwell-like equations against experiments but also to coarse-grained simulations (as it is difficult in experiments to disentangle only one phenomenon from the

overall macroscopic data). Random walk (RW) simulation is used to mimic diffusion[9] without taking into account the interaction of the diffusing probe with t sur une large gamme de he pore walls and without any hydrodynamic drag effect with solvent due the displacement of a molecule of finite size in a pore of finite size. Experimentally, such conditions are difficult to realize even if it is possible to carry out experiments in non-adsorbing conditions with molecules that are small compared to pore size[10]. Here, we compare the predictions from Maxwell's equation with random walk simulations for some simple pore morphologies. The objective is to quantify the porosity ranges where EMT can be applied as a reasonable approximation. This aspect is important as we recall that Maxwell's equation was established for highly diluted spherical inclusions in a continuous medium. As a result, its applicability to concentrated systems remains a questionable approximation.[11] The main throughput of the coarse-grained simulations proposed here is the determination of the tortuosity parameter defined as the ratio of the mean square displacements calculated with and without the porous medium. This is a rigorous mathematical definition that has the advantage to be equivalent to the ratio of diffusion coefficients for the bulk and confined fluid. Such diffusion processes, which correspond to Brownian motion, *i.e.* Fick's diffusion, can be directly compared to diffusion experiments such as NMR and quasielastic neutron scattering. Moreover, tortuosity is accessible by other experiment types, such as electrical conductivity, which makes it a useful parameter to describe the influence of morphology on any type of transport – even if, practically, different values may be obtained with different experimental approaches.[12] Discrepancies have been underlined, for example, between hydrodynamics and conductivity experiments,[12] but a very good agreement is generally observed between conductivity and diffusion experiments for a large number of materials (ranging from simple chromatographic supports to complex structures such as cements).[8,13,14] Diffusion coefficients can be derived from measurement concentration versus time or distance, like in chromatography[15], or in NMR methods.[13,16] The disagreement between different experimental methods may arise from the use of different probes that interact differently with the walls of the porous material. Seen as a topological parameter, tortuosity must be determined in conditions where the probe has negligible interaction with the walls. On another side, the agreement between conductivity and RW simulations has been shown for simple configurations.[17]

In general, tortuosity is not considered as a well-defined parameter in the literature since no common definition has been adopted until now. The basic intuitive mathematical definition as a ratio of the length of the way through the porous medium between two points to the direct distance between these points does not bring any useful information when compared to real phenomena where trajectories explored by molecules obey complex laws that couple Brownian motion and advective flow. In contrast, the RW tortuosity – defined as the ratio of the mean square displacements as underlined above – is a rigorous mathematical definition that is directly related to a physical diffusion coefficient (the self-diffusivity). Moreover, it can be easily shown that other definitions of tortuosity based on conductivity or permeability also correspond to the ratio of distances to the square.[12] Nevertheless, whereas in simulations one can consider a point like tracer with elementary displacements very small as compared to pore size, real experiments are done with finite size probes whose center cannot explore all the void space. Consequently, any experimental tortuosity value based on diffusion or conductivity experiment is an "apparent tortuosity", which gets closer to the "absolute tortuosity "as the probe size decreases. All along this article, the term of "apparent tortuosity" will be kept while the term of "absolute tortuosity" will be restricted to the value obtained by RW simulations. The apparent tortuosity obtained by measurements with the smallest probes should be very close to the absolute tortuosity. It is assumed that the "absolute tortuosity" is a

parameter independent of the experimental method employed and characteristic of morphology effects on transport.

The remainder of this paper is divided in three sections. In the theoretical section 2, the equations used to relate tortuosities at the different scales, RW simulations and model materials built to conduct our study are described. The use of solids reconstructed from tomography methods, based on Xray or TEM , provide a mean to assess transport from realistic numerical porous materials.[18,19] Other considered numerical materials are based on simple shape pores but assembled in a way that mimics the hierarchical structure met in chromatography systems, *i.e.* assembly of porous spherical particles or assembly of porous cylinders. In section3, the experimental approach is described. It consists of probing the diffusion of molecules with various sizes under non-adsorbing conditions in chromatographic columns displaying different structures. The apparent tortuosities are determined as a function of molecular size. In section 4, the results given by Maxwell's equations, combining the tortuosities of domains and that of the whole column, are compared to experimental ones as well as to RW simulations in porous media mimicking real samples. A better understanding of how the tortuosities of various domains combine to yield the total tortuosity of a hierarchical porous material is expected. This may pave the way for the rational design of materials with structures that improve their transport properties.

2. Models and simulation methods

2.1. EMT equations

The porous media considered here are numerical models made up of two domains: large pores between spheres or skeleton and small pores inside spheres or skeleton. Some EMT models are currently used to estimate the diffusion properties (resp. conductivity) of a molecule in a porous material as a function of the diffusion (resp. conductivity) properties in the various domains: Maxwell, Landauer, Garnett, and Torquato models.[7,8,20,21] Initially, Maxwell's equation was introduced to determine the conductivity of a suspension of dilute conducting spheres in a conductive medium. The derivation of this equation is based on the supplementary assumptions that the contribution of spheres is additive and that the limit conditions for conductivity is that of the bulk. It can be written as[6,11]:

$$\frac{\sigma^{eff}-\sigma^0}{\sigma^{eff}+2\sigma^0} = \varphi^p \left[\frac{\sigma^p-\sigma^0}{\sigma^p+2\sigma^0} \right] \tag{1}$$

where σ^{eff} is the effective conductivity of the suspension, σ^0 the conductivity of the conductive medium in which the conductive spheres are dispersed. σ^p and φ^p are the conductivity and volume fraction of the spheres. Some authors[6,21] have proposed to directly write this equation in term of diffusion coefficient by replacing the conductivity by the diffusion coefficient leading to:

$$\frac{D^{eff1}-D_m}{D^{eff1}+2D^m} = \varphi^p \left[\frac{D^p-D_m}{D^p+2D_m} \right] \tag{2}$$

where D^{eff1} is the effective diffusion coefficient of the dispersion, D_m the bulk diffusion coefficient, and D^p the effective diffusion coefficient inside the porous spheres.

3

Following Crank[22], the effective diffusion coefficient "*is the diffusion coefficient of a hypothetical homogeneous medium exhibiting the same steady state behaviour as the two-phase composite*". Consequently, there is a direct equivalence between the effective conductivity of a porous medium determined between two electrodes and the effective diffusion coefficient deduced from the molecular flow due to a concentration gradient ∇C between two reservoirs surrounding the same porous medium. However, it is worth noticing that some authors[5] replace the conductivity by the product of the porosity and diffusivity, i.e. εD. The reason for this substitution arises mainly from the way diffusion coefficients are measured. If the diffusion coefficient is deduced from the spatial repartition of species in the porous medium, like in NMR or peak parking experiments, the effective diffusion coefficient is related to a concentration gradient in the porous medium that is proportional to $\varepsilon \Delta C$, where ε is the total porosity of the system and ΔC the concentration drop of the diffusing species between outside reservoirs as defined above. Consequently, the relationship between the effective diffusion coefficients measured by this second method type and the first one is:

$$D^{eff1} = \epsilon D^{eff2} \tag{3}$$

The distinction between the two definitions lead some authors to coin D^{eff1} as the apparent diffusion coefficient.[23] The tortuosity defined as the ratio between the bulk diffusion coefficient and the effective diffusion coefficient determined by the second method can be considered equivalent to that derived from RW simulations. It is then assumed here that $D^{eff} = D^{eff2}$. In the following, the derived equations are then obtained by replacing the conductivity by the product (porosity) x (diffusivity). By replacing φ^p by $(1 - \varepsilon_e)$, where ε_e is the interparticle porosity, Maxwell's equation expressed in terms of tortuosity can now be written:

$$\tau = \frac{D_m}{D^{eff}} = \epsilon_t[r_m] \left[\frac{1 - (1 - \varepsilon_e)\beta}{1 + 2(1 - \varepsilon_e)\beta} \right] \tag{4}$$

were $\varepsilon_t[r_m]$ is the total porosity accessible to the diffusing molecule of size r_m, τ is the total apparent tortuosity of the column, and $\beta = (\Omega - 1)/(\Omega + 2)$. In the last equation, Ω is defined as:

$$\Omega = \frac{\epsilon_p . D_p^{eff}[r_m]}{D_m} = \frac{\epsilon_p}{\tau_p} \tag{6}$$

Ω is the ratio of the effective diffusion coefficient in the spheres $D_p^{eff}[r_m]$ to the bulk diffusion coefficient D_m, ϵ_p the porosity of spheres and τ_p their tortuosity. With these definitions, the tortuosities determined by conductivity and diffusivity experiments for the same system should coincide:

$$\tau = \frac{D_m}{D^{eff}} = \frac{\epsilon_p . \sigma^0}{\sigma^{eff}} \tag{7}$$

provided the following physicochemical conditions are met: non-adsorbing condisdering and small probe fluids. This has been confirmed experimentally quite often.[12,24]

Bruggeman's equation is an extension of Maxwell's equation where it is now supposed that the limit condition for conductivity (far-field) is the effective conductivity. This is a self-consistent approach where the details of the shape and organisation of domains are omitted (in fact, the domain shape and organization are included in an effective way in the domain size definition *d*). Using the same notation as in equation (1) and considering $\varphi^p = 1 - \varepsilon_e$, Bruggeman's equation for two domains in 3D writes:

$$\varepsilon_e \frac{\sigma^0 - \sigma^{eff}}{\sigma^0 + 2\sigma^{eff}} + (1 - \varepsilon_e) \cdot \frac{\sigma^p - \sigma^{eff}}{\sigma^p + 2\sigma^{eff}} = 0 \tag{8}$$

In this paper, other equations will be tested such as Torquato's model[19]:

$$\tau = \frac{D_m}{D^{eff}} = \varepsilon_t[r_m] \left[\frac{1 + 2(1 - \varepsilon_e)\beta - 2\varepsilon_e \xi_2 \beta^2}{1 - (1 - \varepsilon_e)\beta - 2\varepsilon_e \xi_2 \beta^2} \right] \tag{9}$$

where ξ_2 is the so-called three-point parameter. When $\xi_2 = 0$, Eq. (9) simplifies to Eq. (4). A value of ξ_2 = 0.3277 is used when the particles are in physical contact like in chromatographic columns.[25]

Garnett's model reads[21]:

$$\tau = \frac{D_m}{D^{eff}} = \frac{\varepsilon_t[r_m]}{2} \frac{2(3 - 2\varepsilon_e) + 2\varepsilon_e \Omega}{2(3 - 2\varepsilon_e)\Omega + 2\varepsilon_e} \tag{10}$$

This model ignores the physical contact between the packed particles, *i.e.* the spatial distribution of the bulk eluent matrix surrounding these particles.

Landauer's model reads[26]:

$$\frac{D^{eff}}{D_m} = \frac{a + \sqrt{a^2 + \frac{1}{2}\Omega}}{\varepsilon_t[r_m]} \tag{10}$$

with $a = 1/4 \times [3\varepsilon_e - 1 + \Omega(2 - 3\varepsilon_e)]$

2.2. Random Walk simulations

Porous media construction. Several types of materials were considered to carry out the RW simulations and compare calculated tortuosities with experimental ones. A first set of materials based on the assembly of non-porous particles was built to check quantitatively our simulations against experiments for simple configurations. Moreover, the tortuosity of a compact assembly of non-porous spheres can be used to describe the transport of large molecules that are excluded from particles or skeleton porosity. A second set of materials is made by assembling porous spheres or cylinders, supposed to model chromatographic columns made of spherical particles or of monoliths, respectively. In the case of spherical particles, a first medium is prepared as an assembly of small non-porous spheres with radius *r* in the simulation box enabling to get a porosity ε_i. In this medium a sphere of radius *R* is cut which possesses this internal porosity ε_i. The external porosity is given by the volume between the box and this porous sphere. The simulation is then carried out in an assembly of boxes organized in a cubic configuration. The impact of this specific organization on the results will be discussed later. The external porosity is modulated by modifying the value of *R*. The internal porosity is modulated by varying the radius *r* at constant number of small non-porous spheres. These non-porous spheres are organized also in a cubic arrangement in some cases. For example, a first medium was made of 1728 spheres of diameter 50 in the box 600×600×600 voxels. The internal porosity is 0.476. A second one was made of 1728 spheres of diameter 60. The spheres overlap and the porosity is 0.203. Tests were also done (i) with non-porous spheres in a random configuration prepared as already described[15] and (ii) with a Vycor-like material, built from off-lattice reconstruction based on a TEM image and small angle X-ray scattering[27], in which spheres were also cut. The same procedure was carried out with cylinders made of assembly of non-porous spheres. Crossed-cylinders are considered in a cubic configuration. The various structures are shown in figure 1.
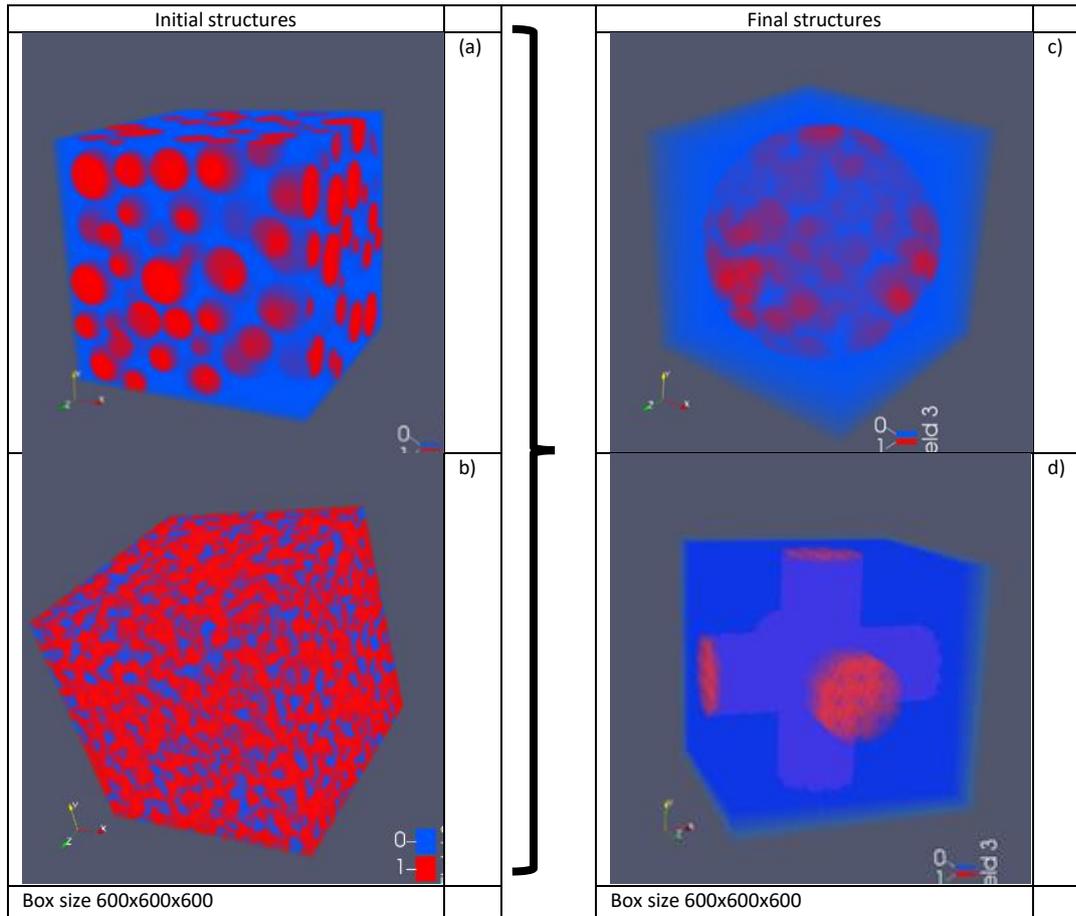
Initial structures		Final structures	
(a)	b)	c)	d)
Box size 600x600x600		Box size 600x600x600	

Figure 1: a) Assembly of non-porous spheres. Random or cubic arrangement of spheres with radius r in a box. Porosity ε_i. r varies from 25 to 36 and ε_l from 0.476 to 0.0268. b) A Vycor like material built from tomography is placed in the box. The resulting porosity is ε_i=0.30. c) A sphere is cut in one of the boxes a) or b) to create a new box with a porous sphere of internal porosity ε_i. The hierarchical material is composed of cubic arrangement of the boxes. External porosity is imposed by the ratio of spheres volume to box volume. d) Crossed cylinders are cut in the boxes a) or b) to create a new box with porous cylinders with internal porosity ε_i. The hierarchical material is composed of cubic arrangement of the boxes. External porosity is imposed by the ratio of cylinders volume to box volume.

Random walk simulation. In this work, the tortuosity τ was calculated by using the random walk method[28,29] as described elsewhere[17]. A porous medium is created based on cubic simulation boxes made of 600×600×600 voxels marked 0 if they belong to the voids and 1 if they belong to the solid phase. Briefly, a "walker" is introduced at random in the pores (voxels marked as 0) and a counter called time t is initialized ($t = 0$). Then, successive displacements are realized randomly. The walker jumps to the next position only if the chosen voxel belongs to the pore space, otherwise a new neighbor is chosen. The counter t is incremented by 1 at every trial. For every t, the squared displacement is calculated from the starting point. This calculation is repeated for a pre-established number of steps. Once the maximum number of steps is reached, a new walker is introduced. When the walker gets out of the box, the walker enters a new box created by periodic conditions. The mean square displacement at each t for N walkers is calculated as:

$$\langle r^2 \rangle = \frac{1}{N} \sum_{i=1}^{N} r_i^2 \tag{12}$$

The tortuosity is calculated at each time t as:

$$\tau = \frac{\langle r^2 \rangle (free\ space)}{\langle r^2 \rangle (porous\ media)} \tag{13}$$

The simulation finishes when the relative error calculated using equation (14) falls below 0.01%.

$$er = \frac{|\tau_{old} - \tau_{new}|}{\tau_{new}} \times 100 \tag{14}$$

The first tortuosity calculations were carried out for simple structures (left column, figure 1) such as that used to build the multiscale porous materials. The results are given in figure 2 where the tortuosities of non-porous spheres or cube assemblies are shown as a function of system porosity. These assemblies can be distributed randomly or organized following face centered cubic (FCC) or body-centered cubic (BCC) structures. Figure 2 also presents the predictions from Weissberg equation[30] that has been experimentally verified on suspensions of spheres by conductivity measurements[24]. Such a comparison allows us to assess quantitatively the validity of our simulation procedure.
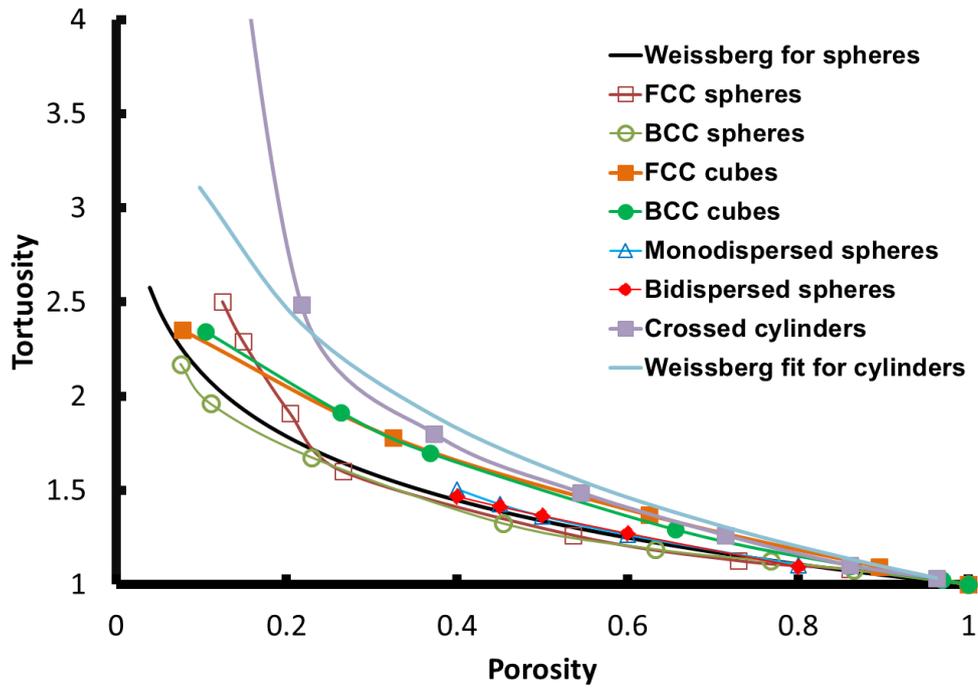

Figure 2: Tortuosity τ calculated by Random Walk simulations for dispersed systems made of the assembly of non-porous particles with simple shapes (see details in the figure). For Monodispere spheres and bidispersed spheres, there is no overlap between the spheres, whereas overlap is allowed for the other configurations

The Weissberg equation reads:

$$\tau = 1 - p\ln(\epsilon) \tag{15}$$

with $p \sim 0.5$ for spheres[24,30,31]. For cubes, a good fit is obtained with $p = 0.65$ in agreement with experimental data.[32,33] For crossed cylinders, the fit using equation (15) for porosities higher than *0.2* yields $p = 0.9$. Below this porosity value, the tortuosity measured by random walk diverges because the percolation threshold is reached. A tortuosity of 6 is obtained for a porosity equal to 0.1. In this cubic arrangement of crossed cylinders (see figure 1d), the percolation threshold corresponds to a porosity of 0.058 if the cylinders are themselves non-porous: this value is obtained by considering in figure 1d crossed non-porous cylinders with a diameter equal to the box size. In the case of FCC or BCC cubes, the percolation threshold corresponds to a null porosity, whereas it is 0.035 for spheres as calculated by considering overlapping spheres with a diameter equal to the diagonal of one face of the simulation box.

These data show two important results. (i) The results agree between simulation and experiment as shown by the results for spheres that can be easily tested experimentally. (ii) In a large porosity range, the tortuosity/porosity relationship depends more on the particle shape than on their arrangement in space since all data for spheres follow the same law, except for porosities lower than 0.2 (regardless of their organized or random distribution and mono/polydispersity). The same behavior is observed for random cubes, but it has been recently shown that, at very low porosity, the behavior for cubes may be different since cubes are oriented if they cannot overlap.[34] For complex structures such as Vycor, a tortuosity value of 3.82 is obtained from RW simulation (whereas experimental values are around 4.2). This is a reasonable agreement since details of surface roughness cannot be assessed by the used reconstruction method so that the reconstructed solid used for RW simulations is probably smoother than the real material.

3. Experimental approach

The diffusion of molecular probes of various sizes in chromatographic columns was studied by means of Peak Parking experiments. Toluene and twelve polystyrene standards (named P1 to P12) with molecular weights M_w ranging between 162 and 1,850,000 g mol^{-1} were dissolved in the mobile phase (THF, Carlo Erba Reagents) at a concentration of 1 g/L. The columns are either composed of fully porous spherical particles made of silica (Lichrospher Si100, Merck) or of a monolithic silica (Chromolith, provided by Merck). The experiments were made by using the 1200 HPLC system (Agilent Technologies), including a quaternary gradient pump with a multi-diode array UV-VIS detector, an automatic sample injector with a 100 µL loop, an autosampler and a thermostated column compartment. The injection volume was set at 1 µL and all experiments were conducted at 298 K. The system is controlled by the Chemstation software.

The peak parking (PP) method was used to measure the apparent diffusion coefficient of molecules through porous media. In the PP experiments, 1 µL of a dilute sample solution was injected at 0.5 mL min^{-1}. The flow is stopped when the solute is supposed to be in the middle of the column and the molecule left to diffuse freely during a given time called the parking time t_p. The flow is then started again at the same value and the peak variance of the solute band is measured by fitting the chromatograms with a Gaussian function. The values obtained without parking are subtracted from the ones obtained with parking. The variance was then plotted versus parking time, and the slope is used to calculate the effective diffusion by using the following equation:

$$D_{eff} = \frac{\Delta\sigma_z^2}{2.t_p} = \frac{1}{2}\frac{\Delta\sigma_t^2}{t_p}\left(\frac{\varepsilon_e}{\varepsilon_t[r_m]}\right)u^2 \tag{16}$$

where u is the interstitial velocity, $\Delta\sigma_z^2$ the variance of the peak in unit of length, $\Delta\sigma_t^2$ that in time. More details on the method and the characteristics of the columns can be found elsewhere.[35] Electrical tortuosity was also determined for comparison by methods already described either for particles or monoliths.[24,35]

4. Results and discussion

Figure 3 shows the apparent tortuosity derived from the effective diffusion coefficient determined by peak parking experiments with the set of non-adsorbing molecules selected here. The data are reported as a function of λ which is the ratio of the molecule size r_m and the average pore size r_p of the small pore domain, i.e. $\lambda = r_m/r_p$. For the smallest molecules, toluene and P1, which have access to the whole porosity, the apparent tortuosity is small: between 1 and 1.25. This agrees with the electrical tortuosity determined on the same samples.[35] Then, upon increasing λ, the apparent tortuosity goes through a maximum before decreasing asymptotically towards a constant value which corresponds mainly to the diffusion of the largest molecules in the large pore domain. Indeed, above λ = 1, polymers are totally excluded from the small pore domain. Clearly, the tortuosity assessed by the largest molecules is that of the large pore domain in which the probe molecule size can be considered small as compared to the pore size (even for large molecules). Indeed, the interparticle pore size of Si100 or the interskeleton pore size in monoliths are in the range 1-3 μm as determined by mercury porosimetry[35] (whereas the size of the largest polymer P12 is around 0.1 μm).[10] In the case of spherical porous particles, Si100, the value for the apparent interparticle tortuosity is 1.38 for an external porosity of 0.376 – in reasonable agreement with the value 1.48 obtained either by RW simulation or by Weissberg equation (14) (assuming p = 0.5). In the case of the monolith, the interskeleton porosity is 0.69 and the measured apparent extraskeleton tortuosity is around 1.05. This value is clearly smaller than that obtained by random walk simulation between crossed cylinders, 1.28, as obtained by extrapolation in figure 2 for the same porosity. This value, which is smaller than expected, but also confirmed by electrical measurements, 1.13 in reference[35], is difficult to understand: the organization of the skeleton is probably very different from that of crossed cylinders used in RW simulations.
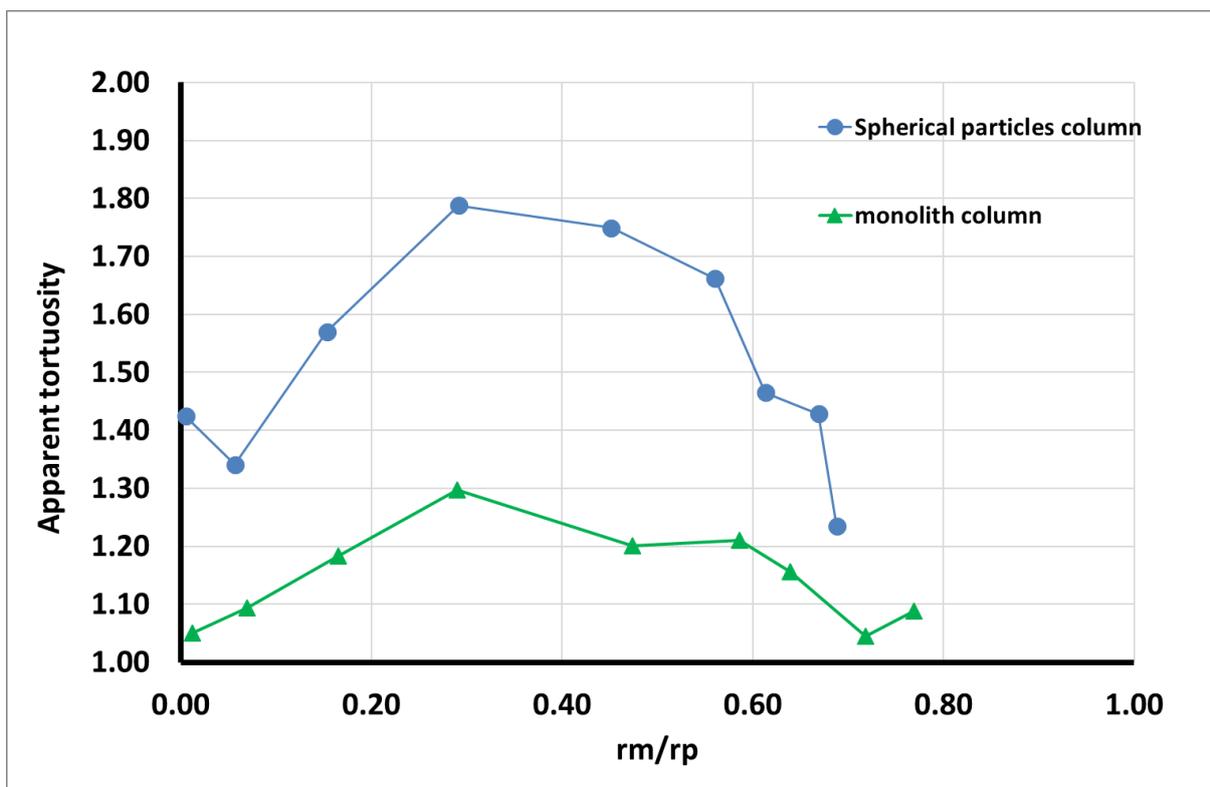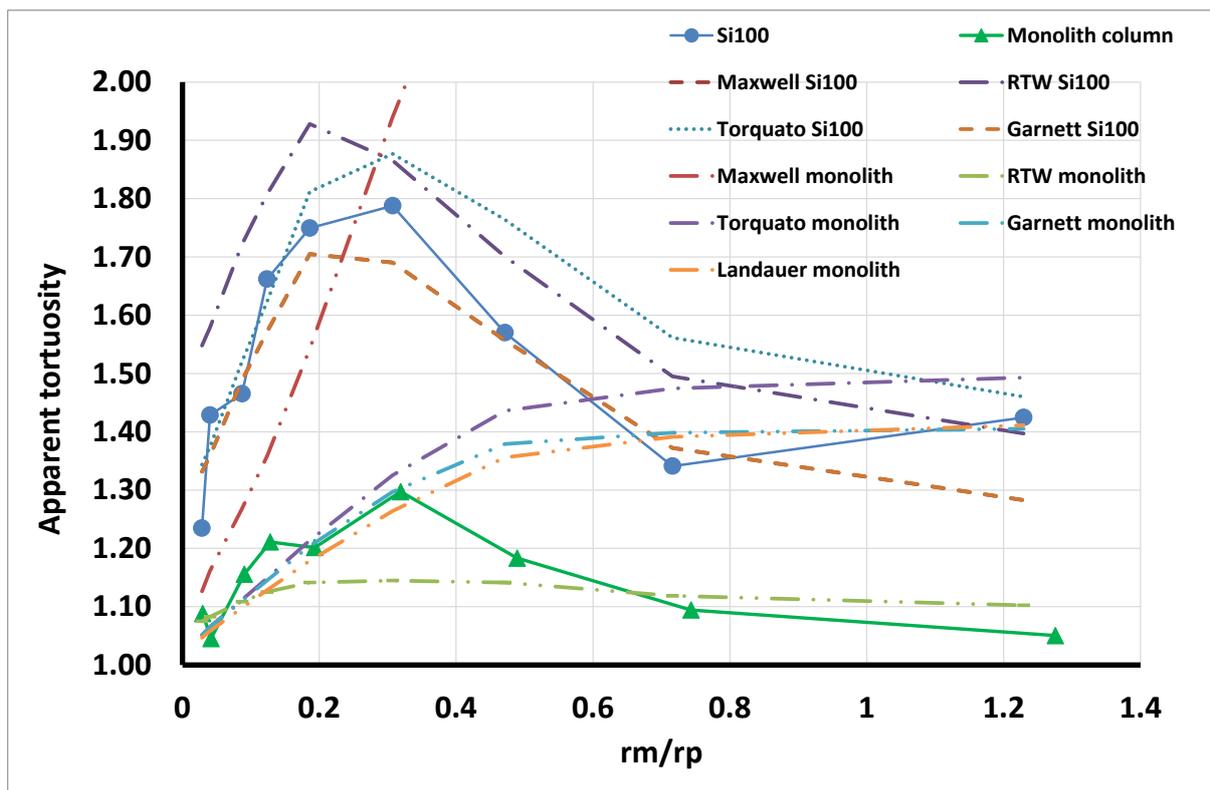
Figure 3: Apparent tortuosity obtained by means of PP method as a function (top) of the ratio between the size of the probe molecule and the small pore domain mean pore size ratio (r_m/r_p) and (bottom) as a function of the accessible internal porosity. Points linked by continuous lines are experimental data.

Broken lines correspond to the different EMT equations indicated in the legends: the calculations are made for the same porosities as in experiments.

The position of the maximum in Fig. 3 is around $\lambda = 0.3$ as already observed for several samples.[35] The apparent tortuosity measured here is the combination of the diffusion behavior of large molecules in large pore and small pore domains. As λ increases, the number of possible ways in small pore domains decreases[36] whereas the proportion of molecules moving only in the large pore domain increases. The description of the process is further complicated by the fact that both the pore size distribution and the polymer sample are polydisperse. Moreover, whereas the diffusion of molecules in the large pore domain can be considered as a simple diffusion mechanism, transport inside the small pore domain is hindered by drag effects because molecule size may be very close to pore size. This phenomenon can be considered by introducing a correction to the diffusion coefficient. This is taken into account for example in the Renkin equation[37] which leads to comparable results with more sophisticated models.[38] Recently, Reich et al[36] proposed a new equation based on random walk simulations in reconstructed pore systems for tracers with different sizes. They established a new empirical equation for the hindrance factor (reverse of apparent tortuosity) as a function of λ. Nevertheless, this equation, which reflects the change of pore accessibility upon varying the probe size, does not consider the drag effect due to the displacement of molecules in a small pore because this drag effect, of hydrodynamic nature, is not considered in RW simulations (in fact, one would have to consider the collective diffusivity to include such collective interactions). This may be the reason why these authors find higher values for the hindrance factor than that obtained previously[8,10] (where the accessibility change with molecular size was described in a less refined fashion but where the drag effect was considered thanks to Renkin's equation). Coming back to the problem of the apparent tortuosity of a multiscale material, the key question here is to disentangle the different contributions to the observed transport. The description of drag effect being complex and out of the scope of this study, the question is to know whether a simple practical description of the effective diffusion in the material can be proposed based on effective diffusivities in each domain. To do so, the EMT equations proposed in the preceding paragraphs were applied and compared to experimental results for the spherical particle column and the monolith. The data are plotted as a function of λ in figure 3a. In the case of spherical particles, the agreement between the experimental data and the theoretical predictions is reasonable on a large range of $\lambda = r_m/r_p$ values (except for Landauer's equation which is not shown here). The simplest EMT model, Maxwell's equation, is accurate enough to describe the apparent tortuosity of a hierarchical material made of a porous sphere assembly. Equations 4 to 7 allow calculating the total tortuosity of the sphere assembly knowing the apparent tortuosity of the spheres. The values of $\tau_p(r_m)$, apparent tortuosity of the polymer with size r_m, used in the calculations are taken from Ref. [35] where they are determined by electrical measurements corrected using Renkin's equation. In applying EMT equations, the transport mechanism (here diffusion) is assumed to be the same in large pore and small pore domains. This is an approximation, especially for small pore domains where the diffusion is hindered by drag effects. One then assumes that the drag effect just modifies the value of the effective diffusion coefficient by a constant factor leading to an apparent diffusion coefficient that is introduced in Maxwell's equation. Despite such an approximation, Maxwell's equation finally captures the results accurately. To test Maxwell's equation in conditions where only diffusion is present, we apply this equation to the data obtained by means of RW simulations. This is done in figure 4 where the RW tortuosities are plotted as a function of total porosity in the case of spherical porous particles for different values of the small pore domain porosity and for different porous structures (sphere or Vycor-like structures). The lines correspond to Maxwell's equation applied using the different porosities,

external and internal, of the structures and the tortuosities τ_p of the small pore domain as determined by RW simulation in the porous structures shown in figure 1.
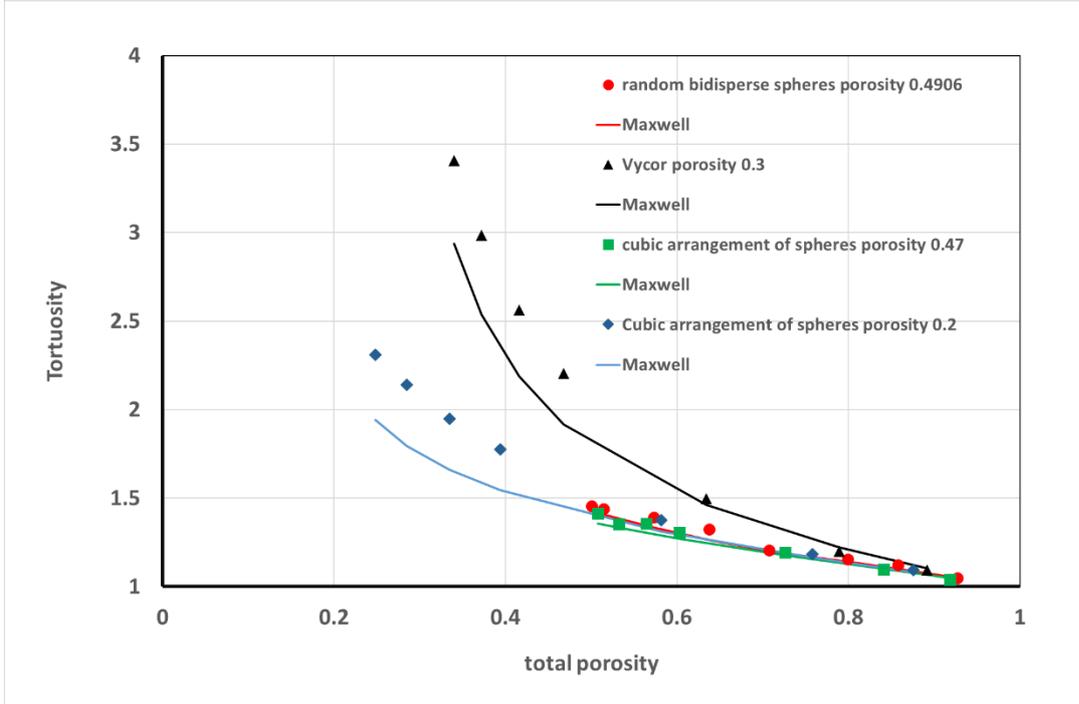

Figure 4: Random walk simulations and predictions of Maxwell's equation for cubic arrangement of porous spheres made of the porous structure indicated in the legend (small pore domain). The total porosity is varied by changing the size of the sphere at constant internal porosity. Only the external porosity is changing.

In figure 5, the same results are presented for the structure made of porous crossed cylinders with two values of the internal porosity of the small pore domain (cylinder made of spheres). Maxwell's equation for cylinders, as often used to describe monolithic materials, is given by[6,7]:

$$\tau = \frac{D_m}{D^{eff}} = \epsilon_t[r_m]\left[\frac{1-(1-\varepsilon_e)\beta}{1+(1-\varepsilon_e)\beta}\right] \tag{17}$$

where $\beta = (\Omega - 1)/(\Omega + 1)$ is different from equation 4. It is important to note that equation (17) corresponds in fact to a 2D arrangement of cylinders with a flow perpendicular to their axis (which is different from the crossed cylinders used in our RW simulations). Nevertheless, despite this strong approximation, the agreement between the simulated data and theoretical predictions remains reasonable. Other configurations have been tested for the arrangement of cylinders, using Maxwell's theory in the case of random cylinders or needles[6]: the agreement remains of the same order. This result suggests that the configuration chosen here is closer to a 2D arrangement of cylinders than to a 3D random arrangement of cylinders when transport properties are considered.
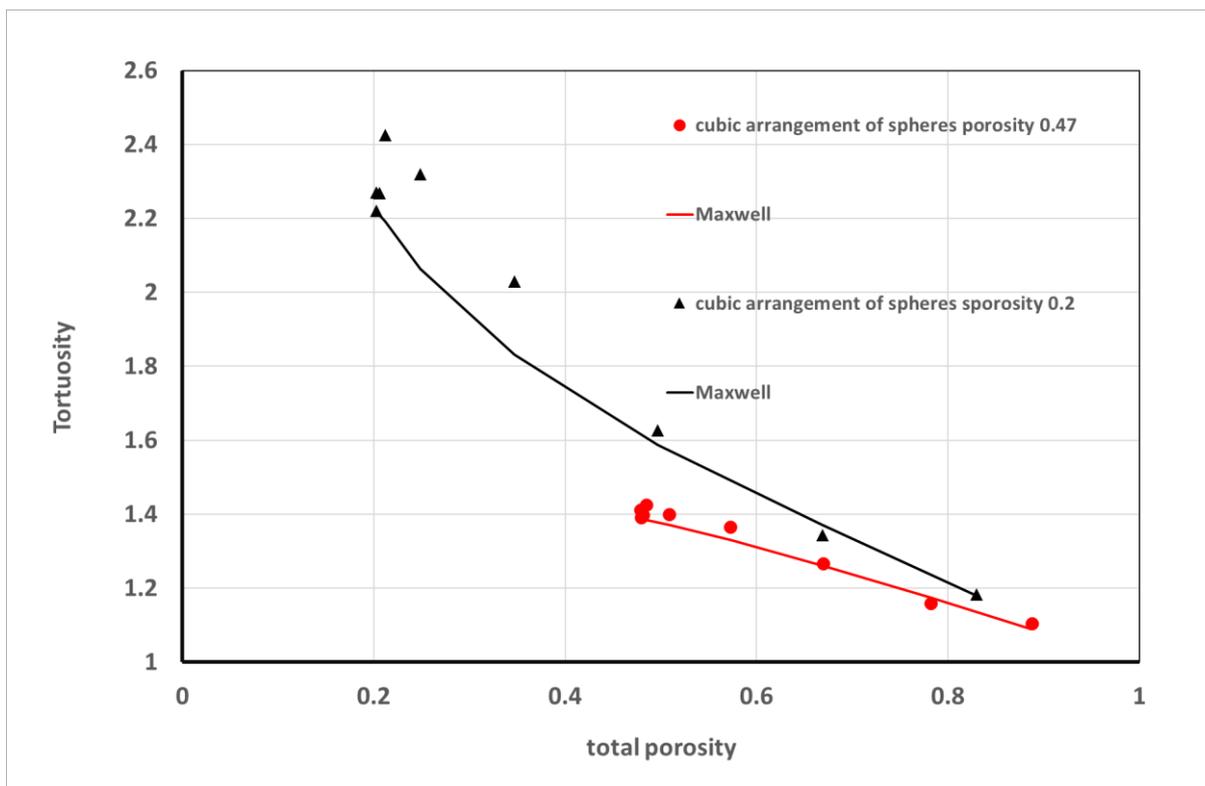
Figure 5: Random walk simulations (symbols) and predictions from Maxwell's equation (thick lines) for crossed porous cylinders made of the porous structure indicated in the legend (small pore domain). The total porosity is varied by changing the size of the cylinders at constant internal porosity. Only the external porosity is modified.

The results above show that Maxwell's equation is a reasonable approximation to predict the tortuosity of hierarchical porous materials in a porosity range that is classical in chromatography. When applying this equation and the corresponding random walk simulation of figures 5 and 6, the tortuosity considered is the absolute tortuosity (as the probe can be considered infinitely small compared to pore size). In contrast, in figure 3, the experimental data correspond to molecules with sizes that are of the same order of magnitude as pore size. As λ increases, the accessible internal porosity decreases. It is thus more appropriate to compare these results to RW simulations at constant external porosity and variable internal porosity. This is done in figure 7 where the RW tortuosity is plotted as a function of internal porosity. The small pore domain is here constructed by considering a cubic arrangement of spheres with increasing size and possible overlap. Like for experimental data in figure 3, a maximum is observed for tortuosity. This maximum is observed at low internal porosities. In the same figure, the results of Maxwell's equation applied to the RW data are shown. The tortuosity is obtained thanks to equations 4-5-6 using the external porosity of the numerical material and the tortuosity of small pore domain obtained by RW simulation. Here again a maximum is obtained in the same porosity range as that obtained using the RW simulation. As for the previously discussed results in figures 4 and 5, the tortuosity obtained using Maxwell's equation is lower than that derived from RW simulations but the evolution with internal porosity is the same. The same figure also reports the results obtained by applying Bruggeman's equation.
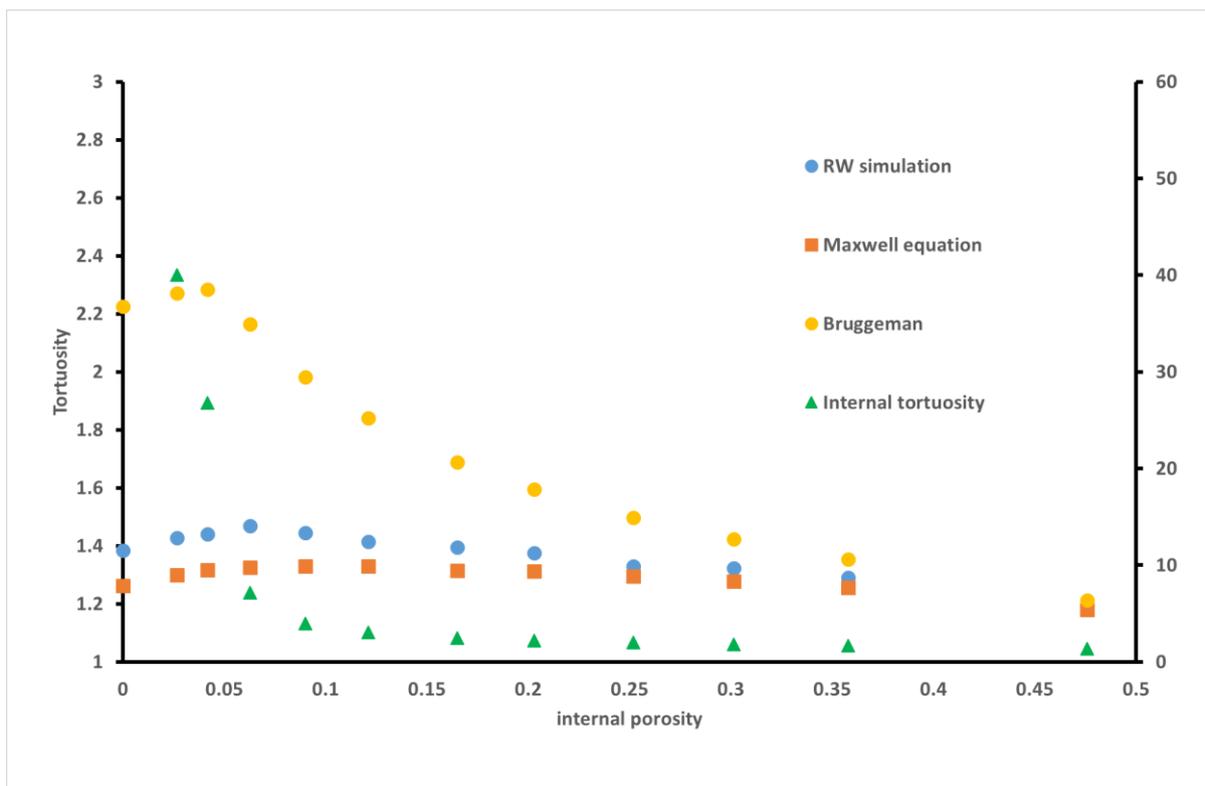
Figure 6: tortuosity of a cubic arrangement of porous spheres as a function of the porosity of the porous spheres. The external porosity is constant and equal to 0.476. The internal tortuosity, obtained by RW simulation, is shown on the right hand axis.

Above a porosity of 0.4, as already noticed, results are in good agreement regardless of the method used. The RW results range between the predictions from Bruggeman and Maxwell equations, with a large overestimation calculated when using the Bruggeman equation. The maxima observed here for the three methods indicate that the observed experimental results for apparent tortuosity in figure 3 can be partly explained by a contribution of pure diffusion without any hydrodynamic effect consideration. Because the experimental maximum is higher than that of the RW simulation or of the Maxwell and Bruggeman models (comparing figures 3 and 6), it indicates that another phenomenon must be considered (*i.e.* the drag effect already introduced above). It can be also observed that the position of the maximum on the internal porosity scale is shifted to small values in the case of the simulation. As already discussed, the drag effect on the one hand and the polydispersity of the polymer probes on the other hand are probably among the reasons why the experimental maximum is located at larger internal porosity than the theoretical one. One can also observe that the maximum, in the case of experiments, is higher for spherical particles bed than for monolith.

The main difference between our experiments and simulations is that the simulated solid is made up of a cubic arrangement of *spheres.* This means that, when the internal porosity is decreased by increasing the size of the non-porous constitutive spheres, the connectivity is not modified (i.e. the number of node and branches in the retraction graph is not modified). In the case of the real materials, a porosity decrease, which is considered as equivalent to increasing the probe size, may lead to a decrease in the connectivity as illustrated in the work of Reich et al[36] on a reconstructed solid

representative of the monolith used here. It is possible that the connectivity loss is different between spherical materials and monoliths when the probe size increases. In order to see whether the shift of the maximum position in figure 3 (see experimental data) as compared to that in figure 6 (RW simulations) can be attributed to the drag effect, Maxwell's equation applied to RW data is modified by replacing $\frac{\epsilon_p}{\tau_p}$ by $\frac{\epsilon_p}{\tau_p}k_f$ in equation (6), where k_f is given by Renkin's equation:

$$k_f \ [r_m]) = 1 - 2.104\lambda + 2.09\lambda^3 - 0.956\lambda^5 \tag{20}$$

This equation is obtained by solving the Navier-Stoke equation for a sphere moving inside a cylindrical tube, keeping the first equations of an infinite set[39], and using the central line approximation, *i.e.* the drag effect is the same whatever the molecule position and equal to the value in the center of the tube. The results are reported in figure 7 where experimental data, RW simulations and Maxwell equation applied to RW data before and after introducing the Renkin correction are shown. To link the RW data to r_m/r_p, the experimental relationship between internal porosity accessible to a given probe and r_m/r_p was used. Without reproducing exactly the experimental data, which is not possible here since the numerical and real materials are different, the comparison in Fig. 7 shows that the shift in the maximum after applying the correction leads to a predicted maximum closer to the experimental one.

Conclusion

Diffusion experiments, effective medium theory calculations and random walk simulations were carried out on hierarchical porous materials composed of two pore domains. The different methods show that the apparent tortuosity versus probe size/pore size ratio graphs display a maximum. Because the maximum is present in our RW simulations, it indicates that it is due to diffusion itself i.e. independently of potential drag effect in pores. This analysis also shows that transport in a hierarchical material can be described using simple effective medium theories such as Maxwell's equation to combine data at different scales (such as tortuosities of small pore and large pore domains) provided porosities are above 0.4. The data at each scale can be obtained either from experimental data or numerical simulations. At low porosities, the agreement is rather qualitative, but introducing the contribution of hydrodynamics phenomena, which mostly influence the small pore domain, simply by adding the Renkin equation to Maxwell equation, allows making closer the position of the maximum between EMT and experiments. Simulations at the nanoscale of these phenomena could be also used to provide an efficient diffusion coefficient in the small pore domain.[40,41,42]
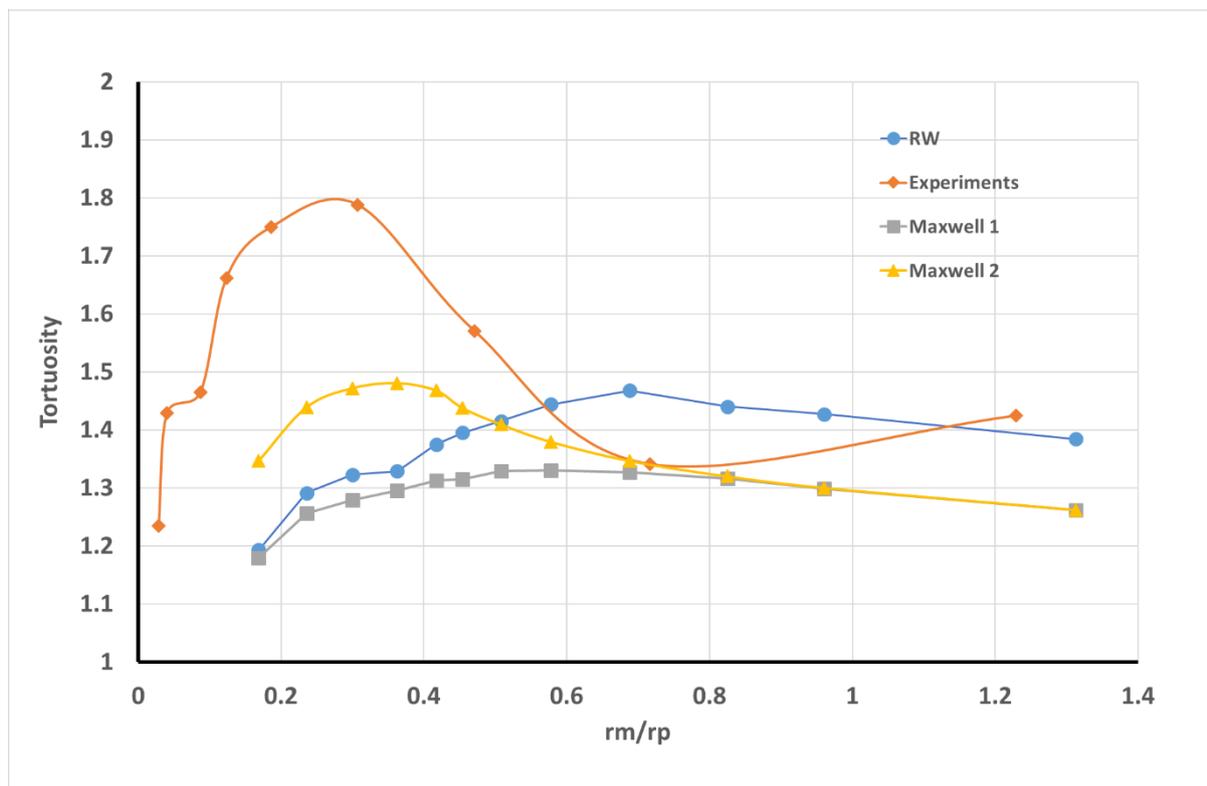
Figure 7: Tortuosity determined by random walk simulation (RW), peak parking experiments (Experiments), Maxwell's equation applied to RW data (Maxwell 1) and Maxwell's equation applied to RW data corrected using Renkin's equation (Maxwell 2). Lines are guide for the eyes.

References

(1) Coasne B.; Multiscale adsorption and transport in hierarchical porous materials (perspective paper), *New J. Chem*. **2016**, 40, 4078-4094.

(2) Volfkovich, Y. M.; Fiippov A. N., and Bagotsky V. S.; *Structural Properties of Porous Materials and Powders Used in Different Fields of Science and Technology*; Springer-Verlag London, **2014**.

(3) Kučera, E.; Contribution to the Theory of Chromatography - Linear Non-Equilibrium Elution Chromatography. *Journal of Chromatography A* **1965**, *19*, 237–48.

(4) Miyabe K.; New Moment Equations for Chromatography Using Various Stationary Phases of Different Structural Characteristics*, Anal. Chem.* **2007**,79, 7457-7472.

(5) Galarneau A.; Guenneau F.; Gedeon A.;, D. Mereib D.; Rodriguez J.; Fajula F.; Coasne B.; Probing Interconnectivity in Hierarchical Microporous/Mesoporous Materials using Adsorption and Nuclear Magnetic Resonance Diffusion, *J. Phys. Chem. C,* **2016**, 120, 1562.

(6) Torquato S.; *Random Heterogeneous Materials*, Springer Science, New York, **2002**.

(7) Desmet G.; Deridder S.; Effective Medium Theory Expressions for the Effective Diffusion in Chromatographic Beds Filled with Porous, Non-Porous and Porous Shell Particles and Cylinders. Part I: Theory. *Journal of Chromatography* A **2011**, *1218*, 32-45.

(8) Wernert V.; Bouchet, R.; Denoyel R ; Impact of the solute exclusion on the bed longitudinal diffusion coefficient and particle intra-tortuosity determined by ISEC. *Journal of Chromatography* A **2014**, *1325*, 179-185.

(9) Deepak P.D.; Bathia S.K.; Transport in Capillary Network Models of Porous Media: Theory and Simulation, Chemical Engineering Science, **1994**, *49*, 245-257.

(10) Wernert V; Bouchet R; Denoyel R ; Influence of Molecule Size on Its Transport Properties through a Porous Medium. *Anal. Chem.* **2010**, 852, 2668-2679.

(11) Maxwell, J. C. *A treatise on electricity and magnetism*; Clarendon Press: Oxford, **1873**.

(12) Ben Clennell, M.; Tortuosity: a Guide through the Maze*, In Developments in Petrophysics*; Lowell, M. A., Harvey, P.K., Eds.; Geological Society Special Publication 122; Geological Society: London, 1997; pp 299-344.

(13) Latour L.L.; Kleinberg R.L.; Mitra P.P. ; Pore Size Distribution and Tortuosity in Heterogeneous Porous Media*. Journal of Magnetic Resonance Science*, Series A **1995**, *112*, 83-91.

(14) Chemni H.; Petit D.; Tariel V. ; Kork J-P. ; Denoyel R. ; Bouchet R. ; Levitz P. ; A Comprenhensive Multiscle Moisture Transport Analysis : from Porous Reference Silicates to Cement-Based Materials. Eur. Phys. J. Spécial Topics **2015**, *224*, 1749-1768.

(15) Knox J.H.; McLaren L.; A New Gas Chromatographic Method for Measuring Gaseous Diffusion Coefficients and Obstructive Factors., *Anal. Chem*. **1964**, *36*, 1477–1482.

(16) Levitz P.; Toolbox for 3D imaging and modeling of porous media: Relationship with transport Properties*. Cement and Concrete Research* **2007**, *37*, 351-359.

(17) Garcia E.J.; Boulet P.; Denoyel, R.; Anquetil J.; Borda G. ; Kuchta B. ; Simulation of Liquid-Liquid interfaces in Porous Media. *Colloids and Surfaces A*, **2016**, *496*, 28-38.

(18) Langford J.F.; Schure M.R.; Yaoa Y.; Maloney S.F.; Lenhoff A.M.; Effects of pore structure and molecular size on diffusion in chromatographic adsorbents. *Journal of Chromatrography A* **2006**, *1126*, 95-106.

(19) Nakashimaa Y.; Nakanoa T.; Nakamuraa K.; Uesugib K.; Tsuchiyamac A,; Ikedad S.; Three-Dimensional Diffusion of Non-Sorbing Species in Porous Sandstone: Computer Simulation Based on X-ray Microtomography Using Synchrotron Radiation. Journal of Contaminant Hydrology **2004**, *74*, 253– 264.

(20) Gritti F.; Guiochon G.; Mass Transfer Kinetics, Band Broadening and Column Efficiency. *J. Chromat. A*. **2012**, *1221*, 2-40.

(21) Torquato S.; Effective electrical conductivity of twophase disordered composite media. Journal of applied Physics 1985, 58, 3790-3797.

(22) Cranck J.; *The Mathematics of Diffusion*, Clarandon Press, Oxford, **1975**.

(23) Baroghel-Bouny V.; Kinomura K.; ThieryM; Moscardelli S.; Easy assessment of durability indicators for service life prediction or quality control of concretes with high volumes of supplementary cementitious materials. *Cement & Concrete Composites* **2011,** *33,* 832-847.

(24) Barrande M.; Bouchet R.; Denoyel R.; Tortuosity of Porous Particles, *Anal. Chem*. **2007**, *79*, 9115.

(25) Gritti F.; Guiochon G.; Experimental validation of physico-chemical models of effective diffusion in chromatographic columns packed with superficially porous particles*. Chemical Engineering Science* **2011**, *66*, 6168-6179.

(26) Landauer R. ; The electrical resistance of binary metallic mixtures. *J. Appl. Phys.* 23 **1952**, *23*, 779.

(27) Levitz P. ; Off-lattice reconstruction of porous media: critical evaluation, geometrical confinement and molecular transport, *Advances in Colloid and Interface Science*, **1998**, 76-77,71-106.

(28) Nakashima Y.; Yamaguchi T.; DMAP. m: A mathematica®program for three-dimensional mapping of tortuosity and porosity of porous media, *Bull.-Geol. Surv. Jpn*. **2004**, *55*, 93–103.

(29) Watanabe Y.; Nakashima Y.; RW3D. m: three-dimensional random walk program for the calculation of the diffusivities in porous media, Comput. Geosci. **2002**, *28*, 583–586.

(30) Weissberg H.L., Effective diffusion coefficient in porous media, *J. Appl. Phys*. 1963, 34, 2636.

(31) Mauret E.; Renaud, M.; Transport phenomena in multi-particle systems—I. Limits of applicability of capillary model in high voidage beds-application to fixed beds of fibers and fluidized beds of spheres. *Chem. Eng. Sci.* **1997**, *52*, 1807-1817.

(32) Wyllie M. R. J.; Gregory A. R.; Fluid Flow through Unconsolidated Porous Aggregates. *Ind. Eng. Chem.* **1955**, *47*, 1379-1388.

(33) Comiti J.; Renaud M.; A new model for determining mean structure parameters of fixed beds from pressure drop measurement application to beds packed with parallelepipedal particles. *Chem. Eng. Sci.* **1989**, *44*, 1539-1545.

(34) Roding M.; Shape-dependent effective diffusivity in packings of hard cubes and cuboids compared with spheres and ellipsoids. *Soft Matter* **2017**, *13*, 8864-8870.

(35) Wernert et al MMM

(36) Reich S-J.; Svidrytski A.; Hlushkou D.; Stoeckel D.; Kübel C.; Höltzel A; Tallarek U.; Hindrance factor Expression for Diffusion in Random Mesoporous Adsorbents Obtained from Pore-Scale Simulations in Physical Reconstructions. *Ind. Eng. Chem. Res*. **2018**, *57*, 3031-3042.

(37) Renkin E.M.; Filtration, diffusion, and molecular sieving through porous cellulose membranes., *J. Gen. Physiol.* **1954**, *38*, 225.

(38) Dechadilok P.; Deen W. M.; Hindrance Factors for Diffusion and Convection in Pores. *Ind. Eng. Chem. Res.* **2006**, *45*, 6953–6959.

(39) Haberman W.L.; and Sayre R.; Motion of rigid and fluid spheres in stationary and moving liquids inside cylindrical tubes. Technical report, DTIC Document, 1958.

(40) Bousige C.; Levitz P. E.; Coasne B.; Bridging scales in disordered porous media by mapping molecular dynamics onto intermittent Brownian motion, *Nature Comm*. 12, 1043 (2021).

(41)Coasne B.; Galarneau A.; Gerardin C.; Fajula F.; Villemot F.; Molecular simulation of adsorption and transport in hierarchical porous materials, *Langmuir* 29, 7864 (2013).

(42) Botan A.; Coasne B.; Pellenq R.; Ulm F. J.; A bottom-up approach of multiscale transport in porous media, *Phys. Rev. E* 91, 032133 (2015).